Monotonic and cyclic crack tip plasticity

L. Guerra-Rosa, C. Moura Branco and J. C. Radon

Monotonic and cyclic plastic zone sizes were measured in a medium strength ferrite-pearlite steel (BM 45) tested in fatigue at 25 Hz at room temperature. Two methods were applied: microhardness and the recently developed 'fatigue in compression' technique. The results obtained are discussed in terms of accuracy and reliability.

The retardation effect due to overloads was also studied in the same material and is illustrated experimentally as a da/dN *vs* ΔK curve. This effect emphasizes the importance of an accurate evaluation of both the size and shape of the overall plastic zone. The shape and dimensions of the cyclic plastic zones seem to indicate that in ductile metals the steady state of fatigue crack growth occurs under plane strain conditions.

Key words: fatigue; microhardness; fatigue in compression; plastic zone characteristics; ferrite-pearlite steels

It is well known that plastic deformation occurring in the vicinity of a fatigue crack tip is sufficient to form a field of residual stresses and frequently to cause a closure.[1] The concepts of residual stress, reversed plastic deformation, crack closure, thickness effect and the differences observed in the plane stress and plane strain situations are familiar factors in fracture mechanics.

Peak loads applied in a constant-amplitude fatigue test may cause crack growth retardation.[2] The prediction of fatigue crack propagation after these peak loads can be based on the size of the plastic zone. However, the retardation of fatigue crack growth caused by a single overload usually does not appear immediately after the overload application but is delayed for a certain number of cycles.[3,4] Some recent detailed studies[5,6] have shown that the shape of the plastic zone may influence not only the fatigue crack propagation rate but also its direction. Therefore, in this paper some particular properties of the monotonic and cyclic plastic zones are discussed. It is hoped that the analysis of the plastic deformation presented may contribute to the fundamental understanding of the mechanism of fatigue crack growth in ductile metals.

The simplest estimate of the dimensions of the plastic zone is based on the original elastic solutions for the stresses at the tip of an ideally sharp crack. Considering a crack loaded only in Mode I and knowing the stress-intensity factor K, it is possible to calculate the distances $r_p^{0^\circ}$ and $r_p^{90^\circ}$, in the planes $\theta = 0^\circ$ and $\theta = 90^\circ$ respectively, where the stress is equal to the yield stress σ_{ys} (Fig. 1). Consequently $r_p^{0^\circ}$ and $r_p^{90^\circ}$ will indicate approximately the plastic zone size. However, it could be assumed that in plane stress ($P\sigma$) the material immediately ahead of the crack tip is homogeneously stressed (*ie* at a stress approximately equal to σ_{ys}) due to the developing of plasticity. This process may be approximated by a tensile test where it has been observed that, if part of the gauge length is more strained than the rest, it hardens in a way that the next increment of strain occurs at another part of the specimen. In the case of crack this increment of strain occurs most probably in the adjacent region further from the crack tip. Additional corrections have to be included as the material ahead of the crack tip has to carry more stress bringing its level close to σ_{ys}. These plasticity effects have been considered by Irwin and others.[6,7]

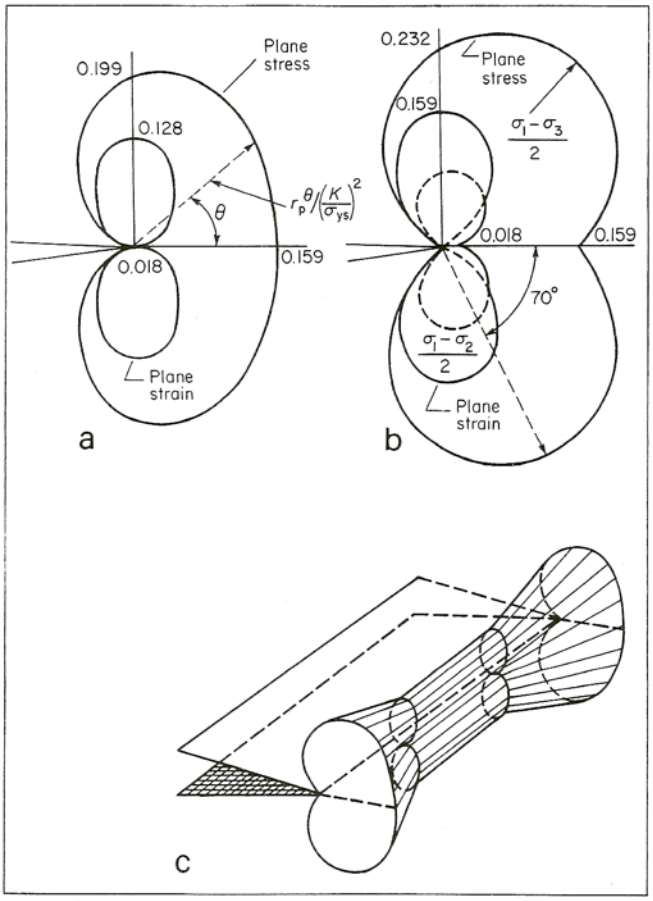

Fig. 1 Plastic zone boundaries as a function of $\alpha = r_p^\theta/(K/\sigma_{ys})^2$ according to (a) Von Mises' criterion, (b) Tresca criterion. (c) Comparison of plane strain and plane stress zones

To examine the yield condition for various θ-angles other than zero, a yield criterion has to be imposed (for example, Von Mises' or Tresca). Fig. 1 shows simplified plastic zone shapes according to these two criteria.

0142–1123/84/010017–08 $3.00

In plane stress ($P\sigma$) the extent of the plastic zone as a function of θ is given by:

Von Mises' criterion:

$$r_p^\theta = \frac{K_{max}^2}{4\pi\sigma_{ys}^2}\left[1 + \frac{3}{2}\sin^2\theta + \cos\theta\right] \quad (1)$$

Tresca criterion:

$$r_p^\theta = \frac{K_{max}^2}{4\pi\sigma_{ys}^2}\left[\cos\frac{\theta}{2}\left(1 + \sin\frac{\theta}{2}\right)\right]^2 \quad (2)$$

As r_p^θ depends on the applied K and σ_{ys} according to the equation:

$$r_p^\theta = \alpha^\theta\left(\frac{K_{max}}{\sigma_{ys}}\right)^2 \quad (3)$$

only the values of the constant α^θ are of interest.

For plane strain ($P\epsilon$), the principal stress $\sigma_3 = \nu(\sigma_1 + \sigma_2)$ and the boundary of the plastic zone as a function of θ is given by Equations (4) and (5):

Using Von Mises' criterion:

$$r_p^\theta = \frac{K_{max}^2}{4\pi\sigma_{ys}^2}\left[\frac{3}{2}\sin^2\theta + (1-2\nu)^2(1+\cos\theta)\right] \quad (4)$$

With the Tresca criterion and for $\tau_{max} = \dfrac{\sigma_1 - \sigma_2}{2}$

$$r_p^\theta = \frac{K_{max}^2}{2\pi\sigma_{ys}^2}\cos\frac{\theta}{2}\left[1 - 2\nu + \sin\frac{\theta}{2}\right]^2 \quad (5a)$$

and for $\tau_{max} = \dfrac{\sigma_1 - \sigma_3}{2}$

$$r_p^\theta = \frac{K_{max}^2}{2\pi\sigma^2}\sin^2\theta \quad (5b)$$

The theoretical shape given by the Tresca criterion will be expressed by Equation (5a) or (5b) depending on the value of τ_{max}, whichever is the greater.

Fig. 1 (a and b) provides a comparison for the plastic zone size estimates in $P\epsilon$ and $P\sigma$ according to both criteria. The plastic zone in $P\sigma$ (the extent of which in the thickness direction is dependent on the thickness) is much larger than in $P\epsilon$ and a simplified pictorial relationship between these two extreme types of the plastic zone can be seen better in Fig. 1c.

Some more accurate plastic zone shape calculations in Mode I have been investigated by a number of authors using finite element methods (FEM). These methods take into account almost any flow rate behaviour due to hardening of the material and can also account for the stress redistribution and unloading that takes place during plastic deformation.

Table 1 summarizes the theoretical estimates of α^θ obtained by different methods.

In the simplest case of constant-amplitude fatigue, as well as the monotonic plastic zone, a cyclic plastic zone will be created. The extent of this cyclic plastic zone is a function of θ and r_c^θ, and can be expressed in terms of the cyclic yield stress, σ_{ys}^c:

$$r_c^\theta = \alpha^\theta\left(\frac{K_{max}}{\sigma_{ys}^c}\right)^2 \quad (6)$$

Table 1. Theoretical α^θ calculations

	$\alpha^{0°}$	$\alpha^{90°}$	Method
Plane stress	0.159	0.179	Elastic solution
	0.318	0.358	Rice[7]
	0.392	–	Dugdale model[6]
	0.159	0.199	Von Mises' criterion
	0.159	0.232	Tresca criterion
Plane strain	0.018	0.129	Von Mises' criterion
	0.018	0.158	Tresca criterion
	0.036	0.138	Levy *et al* using FEM considering a perfectly plastic material[6]
	0.041	~0.150	Rice & Tracey using FEM considering a perfectly plastic material[6]
	0.03–0.04	~0.140	Tracey using FEM but dealing with an isotropic hardening material[6]
	0.007	~0.24	Rice & Rosengren[23] considering a strain hardening exponent $n = 0.05$

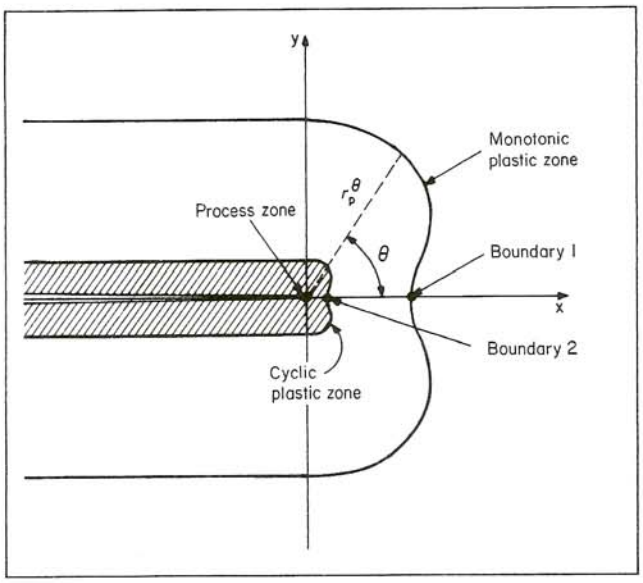

Fig. 2 Schematic drawing of plastic zones around a fatigue crack in plane strain

or in terms of the monotonic yield stress, σ_{ys}:

$$r_c^\theta = \alpha_c^\theta\left(\frac{K_{max}}{\sigma_{ys}}\right)^2 \quad (7)$$

Theoretically, and without taking into account strain hardening, strain ageing and strain rate effects, the cyclic yield stress can be approximated as $\sigma_{ys}^c = 2\sigma_{ys}$, and so the dimensions of the cyclic plastic zone, r_c^θ, will be a quarter of the dimensions of the monotonic plastic zone:[8]

$$r_c^\theta = \frac{r_p^\theta}{4} \quad \text{or} \quad \alpha_c^\theta = \alpha^\theta/4 \quad (8)$$

Using a more detailed analysis and according to Reference 8 the plastically deformed material ahead of the fatigue crack can be divided into three zones (see Fig. 2):

1) A micro-strained plastic zone referred to as the *monotonic plastic zone*. In metals, this zone generally experiences strain cycles in the range $0 < \Delta\epsilon_p < 10^{-3}$. Here $\Delta\epsilon_p$ is the variation of the plastic strain in the y-direction and is continuously increasing.
2) A *cyclic plastic zone*, usually subjected to strain cycles in the range $10^{-3} < \Delta\epsilon_p < 10^{-1}$. $\Delta\epsilon_p$ is also continuously increasing and reaches the value of $\sim 10^{-1}$ at a distance $r^{0^\circ} \approx 0.5$ crack tip opening displacement (CTOD).
3) A very small and highly deformed region located directly in front of the crack tip, called the CTOD-affected zone or *process zone* where the plastic blunting and subsequently the fracture process occur. This third region receives strain cycles with $\Delta\epsilon_p > 10^{-1}$ and its extent is about 0.5 CTOD.

It is noteworthy that the number of cycles that each one of these three zones can receive is independent of the applied ΔK in the steady state of cyclic crack growth (region II of the crack propagation curve). Knowing the dimensions of these three zones and measuring the growth rate da/dN, the number of plastic strain cycles necessary for the instability of each zone may be estimated.

In this paper experimental results of plastic zone sizes are reported and compared with other results available in the literature. A medium strength steel was chosen for the purpose since plastic zone size data are very scarce for this type of material, although it is quite extensively used in fatigue conditions. The objectives of the work were to compare monotonic and cyclic plastic zone size measurements with available theoretical and experimental predictions, to describe overload effects in terms of plastic zone size and also to assess the applicability of the 'fatigue in compression' method for plastic zone size measurement.

Experimental techniques

Several techniques[8–22] (see also Table 4) may be used to measure *in situ* the size of monotonic or cyclic plastic zones such as etching (metallography) and electron channelling patterns (ECP). However in the present work only two techniques were used, microhardness and fatigue in compression.

Material composition and properties

The material used was the medium strength steel BM 45 (CK 45 according to DIN 17200) widely used as a structural steel in machine components. The chemical composition and mechanical properties are given in Table 2.

Table 2. Composition and mechanical properties of BM45 steel

Composition		Properties	
Element	Weight %		
C	0.45	Grain size (μm)	9.2
Mn	0.74	σ_{ys} (0.2% yield stress) (MPa)	335
Si	0.20		
Ni	0.06	σ_{UTS} (MPa)	640
P	0.027	ϵ_{max} (engineering strain at σ_{UTS}) (%)	16.5
S	0.027		
Cr	<0.03	E (MPa)	2.07×10^5

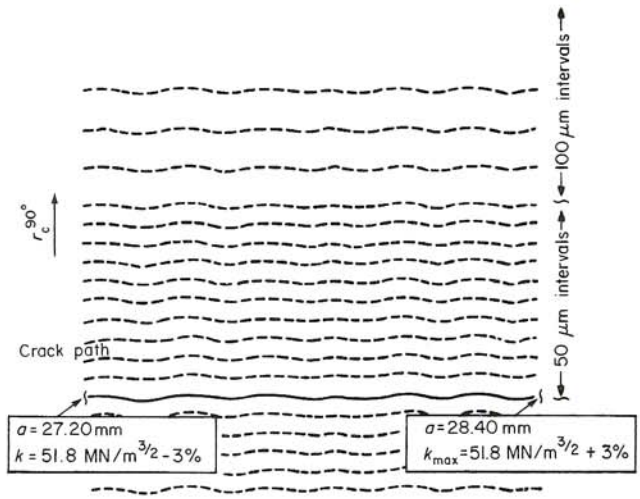

Fig. 3 Schematic arrangement for microhardness measurements

The mechanical properties were obtained in tensile tests at a strain rate $\dot{\epsilon} = 1.85 \times 10^{-3}\ s^{-1}$ using cylindrical specimens with 9 mm diameter and 25 mm gauge length.

Fatigue tests

Fatigue crack propagation tests were conducted according to ASTM Tentative Test Method E647-78T using compact type (CT) specimens. The specimen dimensions were: width (W) 55 mm, thickness (B) 6 mm. Tests were performed in air at room temperature at a frequency of 25 Hz, with a stress load ratio (R) of 0.1, by applying a sinusoidal load wave in a load controlled closed loop electro-hydraulic fatigue testing machine MTS type 811.02. The crack length was monitored with a low power (30x) travelling microscope fitted with a dial gauge. The accuracy of the measuring system was 0.02 mm. Stroboscopic light was used in all measurements and the specimen surface was polished before the tests with 5 μm alumina paste.

Microhardness measurments

Microhardness measurements obtained with a Reichert microhardness system were used to determine the plastic zone sizes. These measurements were made on the surface of one fatigue specimen. The specimen was suitably polished (using 1 μm diamond paste) and etched with 5% Nital. For maximum resolution each indentation was made within one ferrite grain. After preliminary tests a load of 20 gf (0.20 N) was selected as being the minimum load giving an adequate accuracy and repeatability. With this test load the diagonals of the indentations varied from 11 to 15 μm. As the average grain diameter of the material was 9.2 μm only larger ferrite grains were selected in order that both diagonals of the indentation could lie inside the grain.

The microhardness measurements were made at various distances from the crack in a direction normal to the crack plane and restricted to the zone in which the fatigue crack was still closed (r^{90° direction). The applied K_{max} was 51.8 MPa $m^{1/2}$ ± 3%. The measuring equipment at the highest magnification was graduated in 0.16 (6) μm divisions. The indentations were positioned as much as possible near the middle of 50 and 100 μm intervals on both sides of the crack path as shown in Fig. 3. The hardness value attributed to the middle points of each interval was the arithmetic mean of 10 valid observations.

To relate the microhardness values to the stress levels in the plastic zone and to assess the reliability and accuracy of the microhardness technique, a calibration curve HV_{20g} as a function of the true stress $\bar{\sigma}$ was also obtained for the same steel. For this purpose three metallographic samples and 12 cylindrical tensile specimens of 9 mm diameter and 90 mm gauge length were used. The samples and tensile specimens were manufactured from a single rod having the same grain size as the CT specimens. The tensile tests were performed at different stress levels from 15 MPa to a stress slightly above σ_{UTS} with a strain rate of $\dot{e} = 1.85 \times 10^{-3}\ s^{-1}$. The occurrence of necking in one of the specimens was taken into account for the calculation of $\bar{\sigma}$. The microhardness measurements were made on the inside of the tensile specimens (split longitudinally in halves) in the larger ferrite grains by applying the same procedure as in the fatigue CT specimen. The arithmetic mean of the hardness values was also calculated from 10 valid indentations for each stress level.

Fatigue in compression

When a compressive load is applied to a notched specimen the plastic zone at the notch tip will contain residual tensile stresses. Provided the radius of the machined notch tip is as small as possible (*ie* it has a sharp notch tip) and the notch sides do not collapse during the compressive loading, the stress intensity factors at the notch tip can be considered approximately the same as in tension.

After applying a single compressive load P_1 at a corresponding value of K, the specimen is subjected to a cyclic compression varying between 0 and a chosen value P_2, where $|P_2| < |P_1|$. The nucleation and growth of a crack at the notch tip will be observed. This fatigue crack will grow in the notch plane due to the variation of the residual tensile stress existing within the plastic zone created by the previously applied compressive load P_1. The residual tensile stresses alternate between tensile and compressive stresses. The fatigue crack will stop its growth when it reaches a length equal to $r_p^{0^\circ}$ (*ie* the size of the plastic zone corresponding to the original value of K) due to the fading out of the residual tensile stresses.

Once crack growth has stopped, the 'fatigue in compression' test can be discontinued and the specimen is subjected to a tensile test to reveal the fracture surface and identify the area of fatigue crack growth. The shape and size of the fatigue crack in the fracture surface will be that of an intersection of the plastic zone with the plane of the notch, as previously suggested by Reid *et al.*[11]

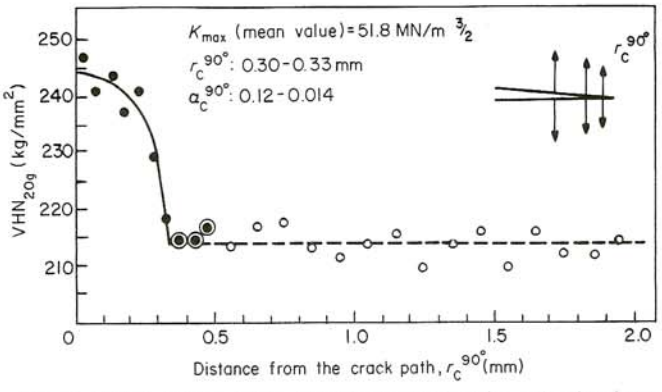

Fig. 4 Cyclic plastic zone size determination by microhardness measurements on the specimen surface of BM 45 steel

Results and discussion

Experimental α^θ and α_c^θ measurements

Fig. 4 shows the results of microhardness measurements obtained on the surface of a CT fatigue specimen 6 mm thick. Only the cyclic plastic zone boundary can be identified ($r_c^{90^\circ}$ = 0.30–0.33 mm) because this technique is not sufficiently sensitive for stress values near σ_{ys} as can be seen from the calibration curve shown in Fig. 5. It may be seen from Figs 4 and 5 that the stress values are considerably higher in the plastic zone, varying between 750 MPa (245 HV_{20g}) and the yield stress.

Tests using the 'fatigue in compression' method were performed on CT specimens of three different thicknesses, 5.95, 19.30 and 24.20 mm. All notch tips were machined using a jewellery saw of 0.2 mm blade thickness. Fig. 6 shows the dimensions of the monotonic plastic zones (in the plane $\theta = 0^\circ$) obtained by this technique.

Table 3 summarizes the α^{0° and $\alpha_c^{90^\circ}$ values obtained from the $r_p^{0^\circ}$ and $r_c^{90^\circ}$ measurements. These results can be compared with the observations reported in the literature[8–22] (see Table 4). This table shows results of α^{0°, α^{90°, (for the monotonic zone) and also the available $\alpha_c^{0^\circ}$ and $\alpha_c^{90^\circ}$ data for the cyclic plastic zones. The values of the ratios $\alpha^{0^\circ}/\alpha_c^{0^\circ}$ and $\alpha^{90^\circ}/\alpha_c^{90^\circ}$ are also included. The plane stress ($P\sigma$) data, Table 4, were also obtained from the measurements on the specimen surface.

Plane strain ($P\epsilon$) results were derived from measurements either at the midplane or at the interior, where a high degree of plane strain was expected.

From the experimental results shown in Tables 3 and 4 it is possible to draw the following conclusions (summarized in Table 5):

1) Plane stress ($P\sigma$):

- the experimental α^{0° value varies between 0.1 and 0.2; the α^{90° value is also within the limits 0.1 and 0.2, excluding the α^{0° and α^{90° values obtained by etching of the Fe-3Si steel. (Measuring plastic zones

Table 3. Experimental α^θ and α_c^θ measurements for BM 45 steel under plane stress

Microhardness technique	'Fatigue in compression' technique				
$\alpha_c^{90^\circ}$	Specimen	Thickness (mm)	Compressive K_{max} (MPa m$^{1/2}$)	$r_p^{0^\circ}$ (mm)	α^{0°
0.012–0.014	CT-X 1	5.95	66.64	7.40	0.187
	CT-A	19.30	55.62	5.10	0.185
	CT-D	24.20	54.20	5.00	0.191
					0.188 (mean value)

by etching is a difficult technique which sometimes may not give very accurate quantitative observations). These data suggest (see Table 1) that the Von Mises' yield criterion or even the elastic solutions give reasonable estimates.

- the ratios $\alpha^{\theta}/\alpha_c^{\theta}$ differ greatly from the theoretical value of 4. A large scatter was observed in these results.

2) Plane strain ($P\epsilon$):

- the α^{0° values range between 0.03 and 0.08. According to Table 1 the best estimates are given by finite element methods but it seems that those methods provide conservative α^{0° calculation. The α^{90° values vary between 0.04 and 0.1, with an average and most frequent value of 0.05 which is approximately one third of the theoretical estimates (see Table 1).
- the scatter obtained in the values of $\alpha^{\theta}/\alpha_c^{\theta}$ in $P\epsilon$ is considerably smaller than in $P\sigma$. All the $\alpha^{\theta}/\alpha_c^{\theta}$ ratios are higher than 4 and the average value of this ratio is approximately 5.

The authors believe that the large scatter found in the $\alpha^{\theta}/\alpha_c^{\theta}$ ratios quoted in the literature and measured at the specimen surface is due to the fact that both α^{θ} and α_c^{θ}

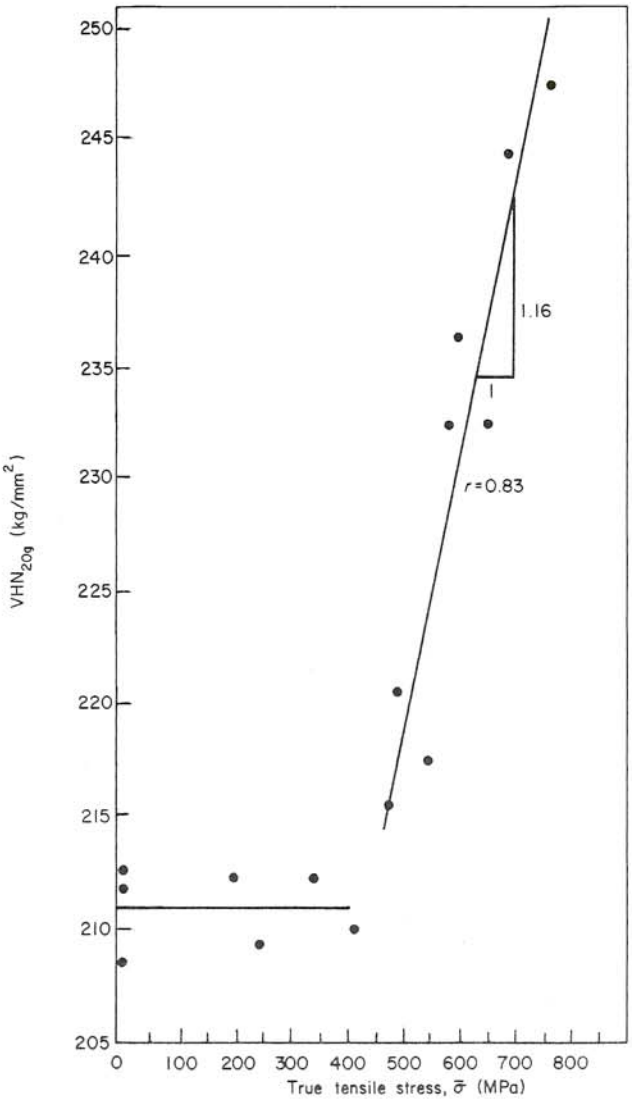

Fig. 5 Variation of microhardness with true tensile stress (calibration curve) for BM 45 steel

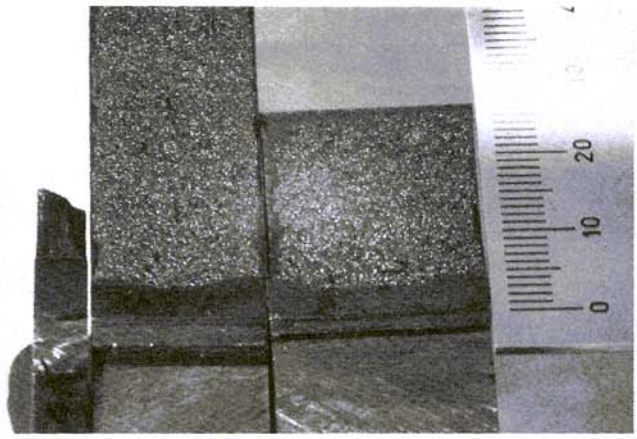

Fig. 6 Monotonic plastic zones (in the plane $\theta = 0^\circ$) revealed by the 'fatigue in compression' technique

were considered under the same state of stress. In fact, the average experimental $\alpha_c^{0^\circ}$ and $\alpha_c^{90^\circ}$ values in $P\sigma$ are respectively 0.008 (excluding the Fe-3Si $\alpha_c^{0^\circ}$ value marked with an asterisk) and 0.012. The corresponding values in $P\epsilon$ are 0.012 and 0.013. In spite of the very few data for $\alpha_c^{0^\circ}$ it may be concluded that all the α_c^{θ} values correspond to plane strain ($P\epsilon$) states. In plane strain the experimental results available in the literature show that in ductile metals the steady state of fatigue crack growth generally follows a transgranular striation mechanism. The striations are normal to the crack growth direction and, at least in region II of fatigue crack growth, each striation corresponds to a load cycle of alternating shear on the planes of maximum resolved shear stress, *ie* slip planes. This type of mechanism and striation orientation is not possible in $P\sigma$ because, for $\theta = 0^\circ$ ($\sigma_1 = \sigma_{ys}$ and $\sigma_3 = \sigma_z = 0$), the maximum (macroscopic) shear stress τ_{max} occurs at planes passing through the x axis at 45° with σ_1 (y direction) and σ_3 (z direction), as indicated in Fig. 7. On the other hand, in $P\epsilon$ both the slip mechanism and the resulting striation orientation are possible. In this case σ_1 and σ_2 have the same magnitude as in $P\sigma$, and $\sigma_3 = \nu(\sigma_1 + \sigma_2)$. In the $P\epsilon$ state, and as shown in Fig. 7, the maximum shear stress occurs on the plates passing through the z axis at 45° with σ_1 (y direction) and σ_2 (x direction).

The effect of overloads

The retardation effect on fatigue crack growth due to a tensile overload was used in the present work to check the validity and application of the plastic zone size calculations.

A fatigue crack propagation test was performed on a CT specimen (dimensions: B = 5.59 mm, W = 54.50 mm) cyclically loaded at 25 Hz in air at R = 0.1. The crack length *vs* number of cycles is shown in Fig. 8. This test was conducted until a crack length of 17.84 mm was reached. At this point (Point P1 in Fig. 8) a single overload of 19 600 N (K = 85.10 MPa $m^{1/2}$) was applied. The fatigue test was then restarted and when the crack length reached 19.61 mm (Point P2 in Fig. 8) another peak load of 9800 N (K = 46.25 MPa $m^{1/2}$) was applied.

Subsequently the fatigue test was continued up to a crack length of 34.20 mm and then stopped.

Based on the experimental α^{0° value previously measured using the 'fatigue in compression' technique it is possible to estimate the extent of the monotonic plastic zones corresponding to each peak load. Assuming a $P\sigma$ condition α^{0° = 0.188, for the 19 600 N peak load:

Table 4. Other experimental α^{θ} and α_c^{θ} – values

	Material	σ_{ys} (MPa)	$\alpha^{0°}$	$\alpha^{90°}$	$\alpha_c^{0°}$	$\alpha_c^{90°}$	$\alpha^{\theta}/\alpha_o^{\theta}$	Technique
Plane stress	Low carbon steel	220	0.07	–	0.007	–	10.0	ECP[9]
					0.009		7.8	XMB[10]
	En 8 steel	350	0.195	–	–	–	–	Fatigue in compression[11]
	304 stainless steel	224	0.144	0.144	–	0.006	24.0	ECP, replication[12]
	Fe-3 Si steel	420	0.10	0.10	–	0.009	11	ECP, replication[12]
	Fe-3 Si steel	460	0.25	0.26	0.0035*	0.017	~70*	Etching[8]
							15	
	Inconel 718	1070	–	0.07–0.09	–	–	–	Etching[13]
	Al 6061-T6	296	0.09	0.14	–	0.016	8.7	ECP, replication[12]
Plane strain	En 8 steel	350	0.035	–	–	–	–	Fatigue in compression[11]
	16-13 stainless steel	193	–	0.05	–	0.012	4.2	Microhardness[14]
	24-20 stainless steel	276	–	0.05	–	0.012	4.2	Microhardness[14]
	301 stainless steel	360	–	0.05	–	0.01	5.0	Microhardness[14]
	Fe-3 Si steel	460	0.034	~0.13	0.008	0.023	4.3	Etching[8]
							5.6	
	Maraging steel	1790	–	0.1	–	–	–	Microhardness[14]
	(annealed)	960		0.06				
	Fe-34 Ni	262	–	0.05	–	0.01	5.0	Microhardness[15]
	Inconel 718	1070	–	0.03–0.05	–	–	–	Etching[13]
	Al – 1/2 Mg	117	0.08	0.08	0.015	0.015	5.3	TEM[16]
	Polycrystalline copper	53	0.056	0.056	0.014	0.014	4.0	Microhardness[17]
	Cu – 2.2 Al	83	–	–	–	0.011	–	Microhardness[17]
	Cu – 1.2 Al	127				0.013		
	Cu – 6.3 Al	138				0.0135		

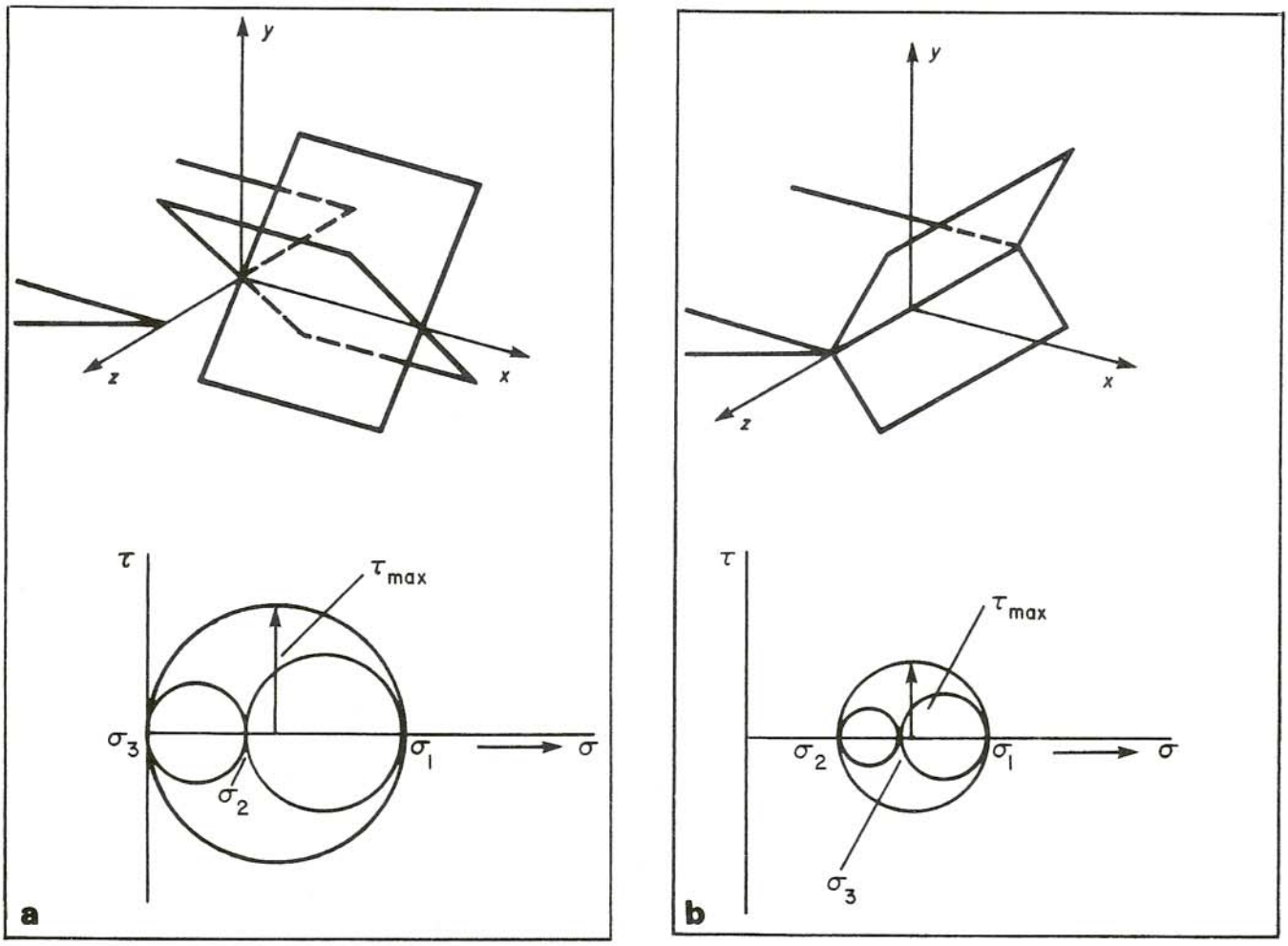

Fig. 7 Planes of maximum shear stress for $\theta = 0$; (a) plane stress, (b) plane strain

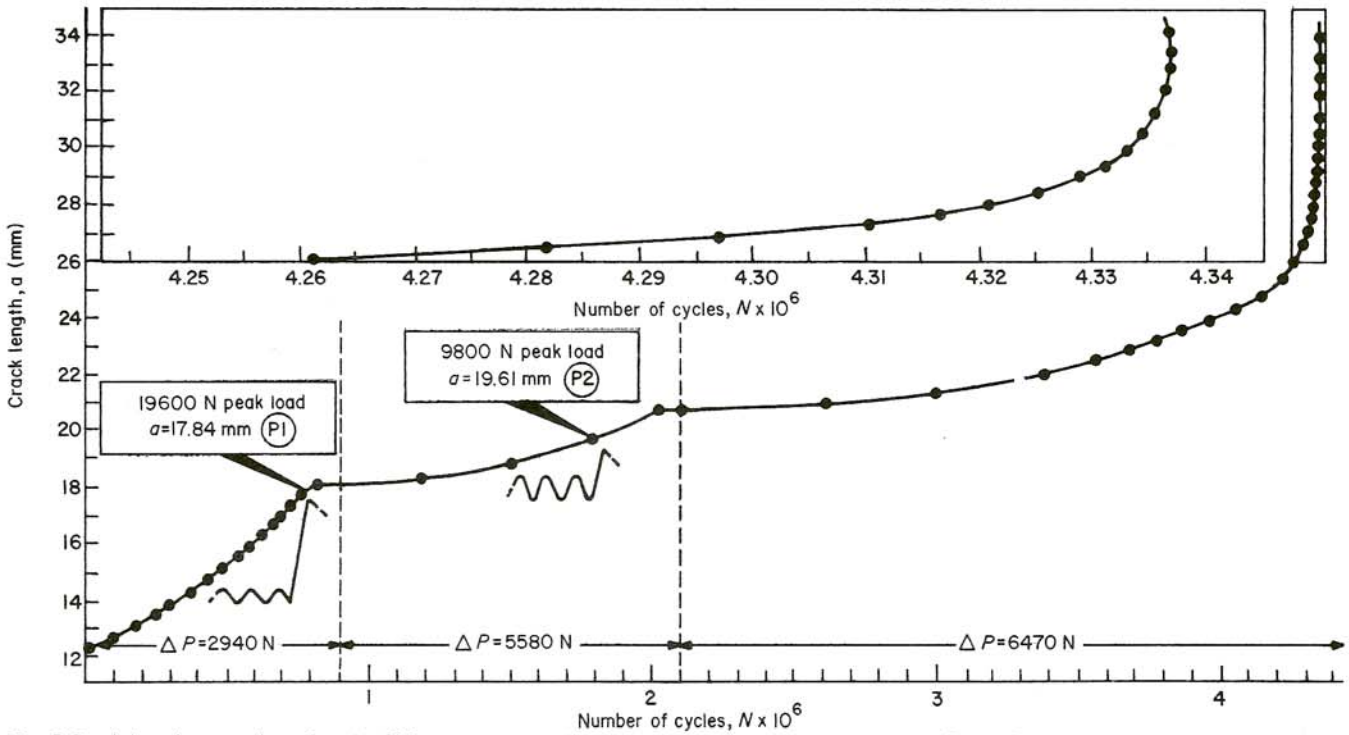

Fig. 8 Crack length *vs* number of cycles N for constant amplitude loading, with peak loads at points P_1 and P_2

Table 5. Summary of experimental α^θ and α_o^θ values

	$\alpha^{0°}$	$\alpha^{90°}$	$\alpha_c^{0°}$ (average)	$\alpha_c^{90°}$ (average)	$\alpha^\theta/\alpha_c^\theta$
Plane stress	0.1–0.2	0.1–0.2	0.008	0.012	Large scatter 7.8–24.0
Plane strain	0.03–0.08	0.04–0.1 (average 0.05)	0.012	0.013	Higher than 4 4.0–5.6

$$r_p^{0°}\ (\text{at P1}) = 0.188 \times \left(\frac{85.10}{335}\right)^2$$

$$= 12.13 \times 10^{-3}\ \text{m} \qquad (9)$$

and for the 9800 N peak load:

$$r_p^{0°}\ (\text{at P2}) = 0.188 \times \left(\frac{46.25}{335}\right)^2$$

$$= 3.58 \times 10^{-3}\ \text{m} \qquad (10)$$

Therefore the monotonic plastic zone created by the 19 600 N peak load at a = 17.84 mm will extend as far as a = 17.84 + 12.13 = 29.97 mm; the monotonic zone corresponding to the 9800 N load (at a = 19.61 mm) will have its boundary at a = 19.61 + 3.58 = 23.19 mm. Hence the monotonic zone for the second overload will be contained within the monotonic zone for the first overload.

Figs 8 and 9 show that the retardation effect appeared after the first overload. Similarly another decrease in crack propagation rate occurred due to the second overload. In spite of a continuously increasing ΔK field some crack growth rates after P2 are lower than the observed da/dN values between P1 and P2. It is clear that the residual compressive stresses within the second overload zone were higher than those existing within the first overload zone. The effect of this second overload was to decrease again the effective ΔK value at the crack tip, ΔK_{eff}.

Figs 8 and 9 also show that the retardation effects did not appear immediately after the application of the overloads. Perhaps the fatigue crack growth rate only decreased when the crack tip process zone reached the boundary of the monotonic zone accompanying the fatigue crack prior to each peak load. An estimate of r_p^0 values, for $P\sigma$ conditions just before the overloads, gives 0.34 mm at P1 and 1.43 mm at P2, agreeing well with the experimental results shown in Fig. 8. The penetration of these $P\sigma$ plastic zones into the interior of the specimen is yet to be determined.

The da/dN values in Fig. 9 were obtained in the constant-amplitude fatigue tests without overloading. The curve shown (solid line) was obtained by fitting a curve to the results of tests conducted on three CT specimens using the same mechanical and environmental conditions. It can be seen that the retardation effect ceases to exist when ΔK in the fatigue (with overloading) test was approximately 55 MPa $m^{1/2}$. In that test, this ΔK value corresponded to a crack length of 30.6 mm, confirming the previously estimated position of the overall plastic zone boundary (a = 29.94 mm).

Conclusions

1) The microhardness technique is not accurate enough to obtain monotonic plastic zone sizes in a ferrite-pearlite steel (BM 45) with a small grain size. However, if this technique is properly used the size of the cyclic plastic zone in a direction normal to the fracture plane, $r_c^{90°}$, can be found.
2) The 'fatigue in compression' technique allows a very accurate determination of monotonic zone sizes but only in the $\theta = 0^0$ direction. A direct observation of the plastic zone profile can be made as a projection into the notch plane. This technique looks very promising for plastic zone size measurements and requires further development.
3) An analysis of experimental results obtained in the literature showed a good agreement for the values of

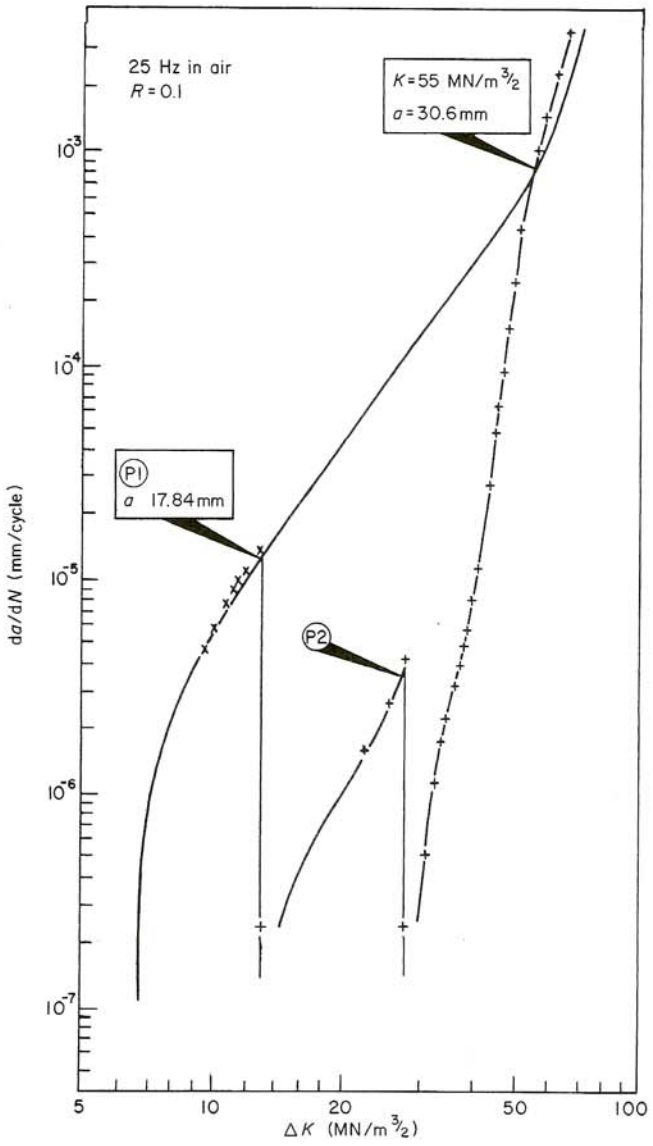

Fig. 9 da/dN *vs* ΔK curves with and without overloading for BM 45 steel

α_c^{θ}, the coefficient of the cyclic plastic zone size. Therefore, taking into account the plasticity criteria for the striation mechanism, it is clear that, in steady state fatigue crack growth in ductile metals, the cyclic zone is always generated and developed under plane strain conditions.

4) Fatigue crack growth rates measured under constant-amplitude conditions applying single and periodic overloads confirm the existence of delayed retardation and the overall plastic zone estimates.

Acknowledgements

The authors gratefully acknowledge the experimental facilities provided by Departamento de Metalurgia and Metalomecânica of L.N.E.T.I. (Sacavém – Portugal).

References

1. **Guerra-Rosa, L. and Branco, C. M.** 'Application of fracture mechanics to corrosion fatigue, Part III' *Tecnometal* No 22 (Oporto, September/October 1982) pp 17–28
2. **Radon, J. C.** 'Stress biaxiality effects on slow crack growth in PMMA' *Advances in Fracture Research* (Pergamon Press, 1981) **2** pp 1109–1126
3. **Matsuoka, S. and Tanaka, K.** 'Influence of stress ratio at baseline loading on delayed retardation phenomena of fatigue crack growth in A553 Steel and A5083 Aluminium Alloy' *Eng Fract Mech* **11** (1979) pp 703–715
4. **Furuya, Y. and Shimada, H.** 'Fracture crack tip strain loop under single overload in Fe-3Si steel' *Eng Fract Mech* **16** (1982) pp 295–301
5. **Lankford, J. and Davidson, D. L.** 'Fatigue crack tip plasticity associated with overloads and subsequent cycling' *J Engng Mat Tech* **98** (1976) pp 17–29
6. **Lankford, J., Davidson, D. L. and Cook. T. S.** 'Fatigue crack tip plasticity' *ASTM STP 637* (1977) pp 36–55
7. **Rice, J. R.** 'Mechanics of crack tip deformation and extension by fatigue' *ASTM STP 4.15* (1967) pp 247–311
8. **Hahn, G. T., Hoagland, R. G. and Rosenfield, A. R.** 'Local yielding attending fatigue crack growth' *Met Trans* **3** (1972) pp 1189–1202
9. **Davidson, D. L., Lankford, J., Yokobori, T. and Sato, K.** 'Fatigue crack tip plastic zones in low carbon steel' *Eng Fract Mech* **12** (1976) pp 579–585
10. **Yokobori, T., Sato, K. and Yaguchi, H.** 'Reports of the Research Institute for Strength and Fracture of Materials' (Tohoku University, Sendai, Japan, 1973) **9.1** pp 1–10
11. **Reid, C. N., Williams, K. and Hermann, R.** 'Fatigue in compression' *Fatigue Engng Mater Struct* **1** (1979) pp 267–270
12. **Davidson, D. L. and Lankford, J.** 'Plastic strain distribution at the tips of propagation fatigue cracks' *J Engng Mat Tech* **98** (January 1976) pp 24–29
13. **Clavel, M., Fournier, D. and Pineau, A. G.** 'Plastic zone sizes in fatigued specimens of INCO 718' *Met Trans* **6A** (1975) pp 2305–2307
14. **Bathias, C. and Pelloux, R. M.** *Met Trans* **4** (1973) pp 1265–1273
15. **Pineau, A. G. and Pelloux, R. M.** 'Influence of strain-induced martensite transformations on fatigue crack growth rate in stainless steels' *Met Trans* **5** (1974) pp 1103–1112
16. **Wilkins, M. A. and Smith, G. C.** 'Dislocation structures near a propagating fatigue crack in an Aluminium – 0.5% Magnesium alloy' *Acta Met* **18** (1970) pp 1035–1043
17. **Saxena, A. and Antolovich, S. D.** 'Low cycle fatigue, fatigue crack propagation and substructures in a series of polycrystalline Cu-Al alloys' *Met Trans* **6A** (1976) pp 1809–1828
18. **Davidson, D. L. and Lankford, J.** 'Fatigue crack tip plastic strain in high-strength aluminium alloys' *Fatigue Engng Mater Struct* **3** (1980) pp 289–303
19. **Wanhill, R. J. H.** 'Environmental fatigue crack propagation in Ti-6Al-4V sheet' *Met Trans* **7A** (1976) pp 1365–1373
20. **Lal, K. M. and Garg, S. B. L.** 'Plastic zones in fatigue' *Eng Fract Mech* **13** (1980) pp 407–412
21. **Chalant, G. and Remy, L.** 'A metallographic method for determining plastic strains at the tip of a fatigue crack' *Mat Sci and Eng* **50** (1981) pp 253–261
22. **Chalant, G. and Remy, L.** 'Plastic strain distribution at the tip of a fatigue crack. Application to fatigue crack closure in the threshold regime' *Eng Fract Mech* **16** (1982) pp 707–720
23. **Rice, J. R. and Rosengren, G. F.** 'Plane strain deformation near a crack tip in a power law hardening material' *J Mech Phys Sol* **16** (1968) p 1

Authors

Both L. Guerra-Rosa and Dr C. M. Branco are with the CEMUL – Centro de Mecânica e Materiais da Universidade Técnica de Lisboa, Instituto Superior Técnico, 1096 Lisboa Codex, Portugal. Dr J. C. Radon is with the Mechanical Engineering Department, Imperial College of Science and Technology, London.